ISBN: 978-3-95450-233-2 ISSN: 2673-5504 doi:10.18429/JACoW-SRF2021-TUPCAV015

PERFORMANCE OF A LOW FREQUENCY QWR-BASED SRF GUN*

G. Chen†, T. Petersen, M. P. Kelly, M. V. Fisher, M. Kedzie, T. Reid, ANL, Lemont, Illinois, USA
X. Lu, P. Piot, Northern Illinois University, DeKalb, Illinois, USA

Abstract

Superconducting radio-frequency (SRF) electron guns are generally considered to be an effective way of producing beams with high brightness and high repetition rates (or continuous wave). In this work, the 199.6 MHz quarter wave resonator (QWR)-based Wisconsin Free Electron Laser (WiFEL) superconducting electron gun was recently refurbished and tested at Argonne (ANL). The field performance of the e-gun was fully characterized. During this time, multipacting (MP) conditioning was performed for over 20 hours to overcome the hard MP barrier observed in the accelerating voltage range of 8 to 40 kV; the presence of multipacting is expected to operationally important for future e-guns. Here we simulated and studied the effect using CST [1] Microwave Studio and Particle Studio and compare with the measured data.

INTRODUCTION

For the next generation light source (such as for the LCLS-II project at SLAC) or the instruments for ultrafast electron diffraction or microscopy, high brightness electron beams are of the high importance, where beam brightness is related to the ratio of the beam current to the emittance. The electron beam source should also achieve high repetition rates (up to continuous wave CW operation), and very short pulses. A promising solution uses a quarter wave superconducting electron gun, which could provide electrons in continuous wave mode, and the cryogenic environment may reduce the normalized transverse emittance of the beam [2].

The 199.6 MHz quarter wave resonator (QWR)-based Wisconsin Free Electron Laser (WiFEL) gun cavity was originally designed and fabricated by University of Wisconsin and NIOWAVE Inc. The cavity was transported and arrived at Argonne for additional tests in December 2019. Due to a damaged coupler bellows and contamination in the cavity, the gun was dissembled and cleaned by high pressure rinsing (HPR), followed by clean re-assembly after the cavity had been fully dried.

The cavity geometry together with the electromagnetic field distributions are presented in Fig. 1. In this work, the MP conditioning process (in CW mode) of the WiFEL cavity was experimentally measured and its behavior was then studied using CST simulations. After breaking through the MP barrier, a sequence of rf cold tests were performed after individual rounds of pulsed conditioning with up to 4 kW of available power. An intrinsic cavity factor Q_0 was found to be 2.3×10^8 at the highest stable CW peak field level of 15 MV/m.

* This work was supported by the U.S. Department of Energy, Office of Nuclear Physics, under Contract No. DE-AC02-06CH11357.
† b288079@anl.gov

The geometry of the WiFEL cavity together with the electromagnetic field distribution is shown in Fig. 1, which is simulated by using the CST Microwave Studio's Eigenmode solver.

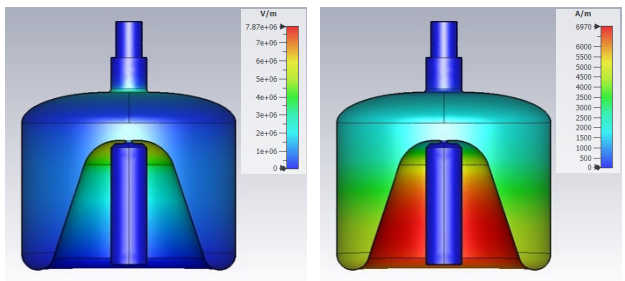

(a) Electric field (b) Magnetic field

Figure 1: Simulated electromagnetic field distribution of the cavity.

CAVITY COLD TESTS

The experimental setup for the cold tests is shown in Fig. 2, where the cathode stalk was replaced by a capacitive cavity field probe with a simulated Q_{ext} of $\sim 1 \times 10^{11}$. The cold tests were started with a 3-day CW MP conditioning until the MP barrier 'broke though'. More studies on the WiFEL cavity's MP behavior will be presented in the next section. Then the cavity Q-curve was determined from the direct measurements of the forwarded (V_F), the reflected (V_R) and the transmitted (V_T) signal voltage in CW mode; two systematic readout errors of ± 0.08 dB from the oscilloscope (Tektronix TDS-7404B) and ± 0.05 dB from the power meter were considered in all measurements.

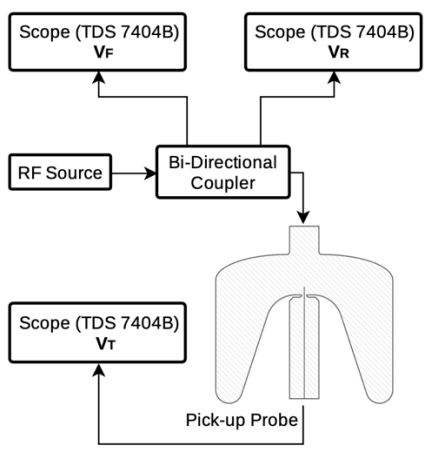

Figure 2: Simplified schematic diagram of the experimental setup.

Figure 3 shows the four Q-curve measurements as a function of the peak gradient (E_{peak}). The first Q-curve was obtained after breaking though the MP barrier. Then

ISBN: 978-3-95450-233-2 ISSN: 2673-5504 doi:10.18429/JACoW-SRF2021-TUPCAV015

some RF pulse conditioning was performed with a duty cycle <5% using up to 4 kW of available power. Following with a sequence of the high-power pulse conditioning, the highest peak field was improved to ~15 MV/m after a third round of pulse conditioning at 4.2 K; additionally, the x-ray radiation was measured simultaneously using an ionization chamber located 1 meter from the cryostat. The measurable x-rays due to the field emission were observed at the field level of 10.6 MV/m, the same level where the cavity Q starts degrading.

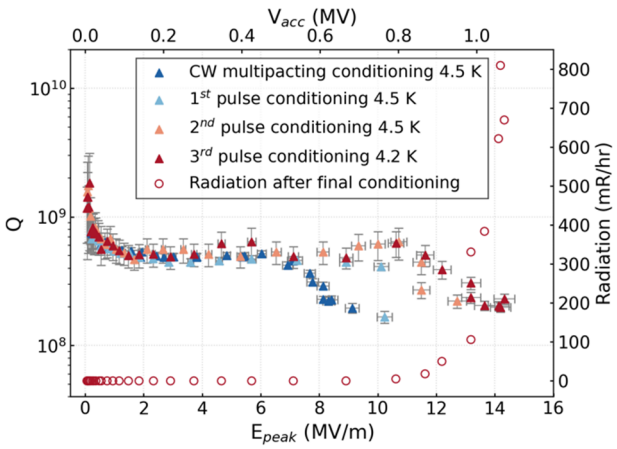

Figure 3: Measured Q curves as a function of E_{peak} (and V_{acc}) are shown in triangles. The radiation data (open circles) were obtained during the Q measurement of "3rd pulse condition 4.2 K".

A Q-drop at low gradient was noticed. To investigate whether this drop was from Q disease, *i.e.* the formation of the lossy surface hydrides during the slow cool-down process, the cavity was warmed up to ~120 K and held there for 4-5 days. More discussion on this can be found in the paper of T. Petersen *et al* [3]. Based on the Q-curve remeasurement, Q-disease was ruled out as the primary cause, and this Q-degradation is more likely related to the physical imperfection (*i.e.* welding defects) on the cavity surface.

MULTIPACTING CONDITIONING

For real SRF cavities, multipacting conditioning is an important process in order to achieve operationally relevant accelerating voltages. The relative MP regions in the cavity and the approximate turn-on gun voltage deserve our attention. Furthermore, in the SRF gun application, the scattering between the secondary emitted particles and the cathode may lead to the degradation in the quantum efficiency (QE), and also to undesired cavity contamination [4].

Experimental Measurements

Figure 4 shows the complete process of the MP conditioning after the cavity re-assembly. Initially the MP conditioning was performed with the coupler full-out at nearly critically coupled condition, where the Q_{ext} was experimentally determined to be 8×10^8 based on the direct measurements of the forward and reflected powers. A strong MP was observed in between about 8 to 40 kV, and it requires 3 days to condition given the parameters of our experimental setup.

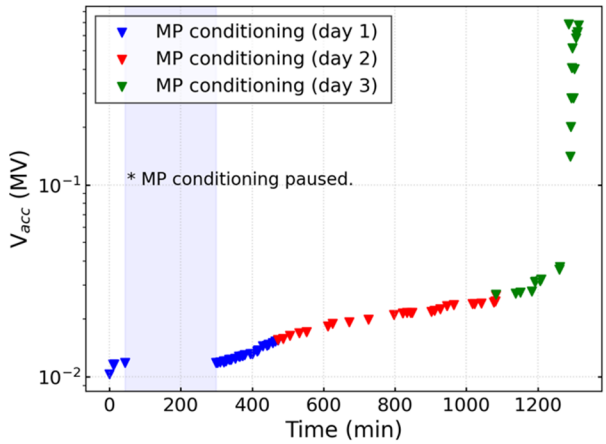

Figure 4: MP conditioning process.

Multipacting Studies by CST

Specific surface conditions of the cavity could greatly contribute to the multipacting effect; possible factors include the presence of the oxide [5, 6], the introduction of impurities to the cavity material and the presence of adsorbed water [6]. Typically, the secondary electron yield (SEY) is the relevant property used to describe bulk materials.

Figure 5 shows three different SEY curves of Nb which were used in the MP simulation; the curve with a SEY_{peak} at 1.5 [5], and the two curved with 1.9 and 2.2 peaks were scaled upward to address different Nb conditions.

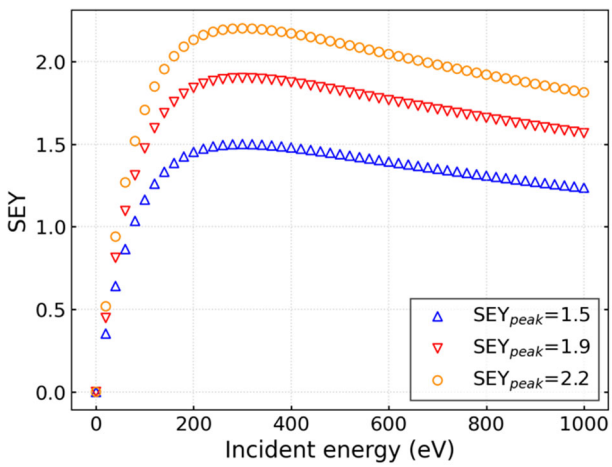

Figure 5: Secondary emission yield curves of bulk Niobium used here and having different peak values.

Our MP simulations were performed using CST Particle Studio's Particle in Cell (PIC) solver with the imported EM field distribution generated by the CST Microwave Studio Eigenmode solver. As shown in Fig. 6, the initial particles are assigned at all surface of the copper coupler and the pick-up probe. To reduce the computational load for this cylindrically symmetric geometry, instead of assigning the initial particles everywhere on the cavity surface, a 45°

ISBN: 978-3-95450-233-2 ISSN: 2673-5504 doi:10.18429/JACoW-SRF2021-TUPCAV015

slice was picked from the cavity surface [4]; this method reduces the number of the initial emission sites by more than 80% and, therefore, effectively lowers the program running time while exploring the same parameter space. The assigned primary particles were emitted within the first rf period (5 ns) with a Gaussian distribution and an assumed kinetic energy of 4 eV.

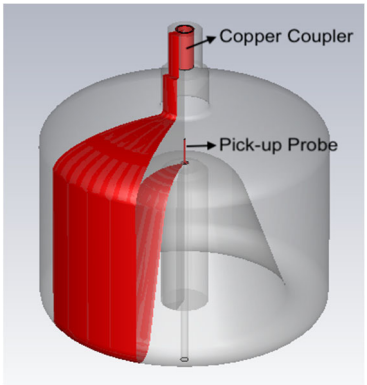

Figure 6: The red region shows the assigned initial particle distribution for MP simulation.

To investigate the experimentally observed strong MP behavior, the MP simulations were performed in between 5 to 45 kV with a step size of 5 kV for three SEY curves to represent different conditions of the cavity surface (Fig. 7 (a)-(c)).

To quantify the particle growth trend in a simple way, the total number of particles (N_e) can be fitted to an exponential function with respect to time:

$$N_e(t) = N_0 e^{\alpha t} \quad (1)$$

where, N_0 is the primary number of particles generated within the first rf cycle, and α is the particle growth rate. By fitting all curves in Fig. 7 to Eq. (1), the growth term α for each curve can be determined individually. A negative α indicates a decrease of the total number of particles, in another words, no multipacting. For a positive α, the higher the value the more particles are generated.

As shown in Fig. 8, for the Nb with a SEY curve having the peak at 1.5 (orange bars), α is less than 0 in the entire accelerating voltage range which suggests no MP effect. As the peak value of SEY curve increases to 1.9 (pink bars) and 2.2 (purple bars), a positive α is found, and the estimated MP turn-on voltages (the intersect with the horizontal 0 line) are found to be ~20 kV and ~ 16 kV, respectively. Based on the trend line in Fig. 8, Nb with a higher SEY is likely having a lower MP turn-on voltage (or a lower barrier).

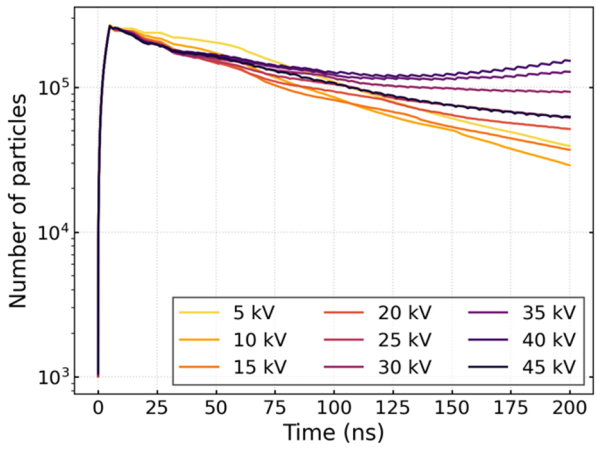

(a) $SEY_{peak} = 1.5$

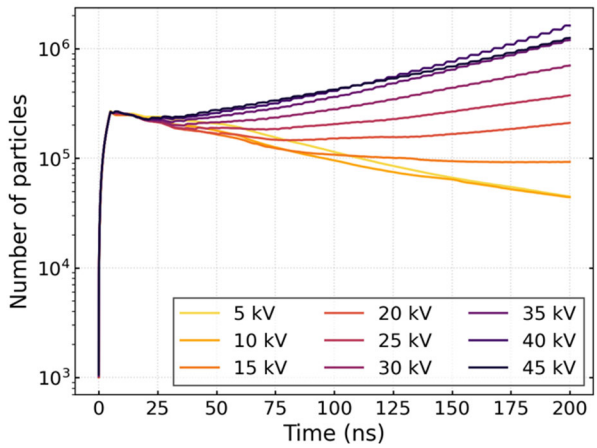

(b) $SEY_{peak} = 1.9$

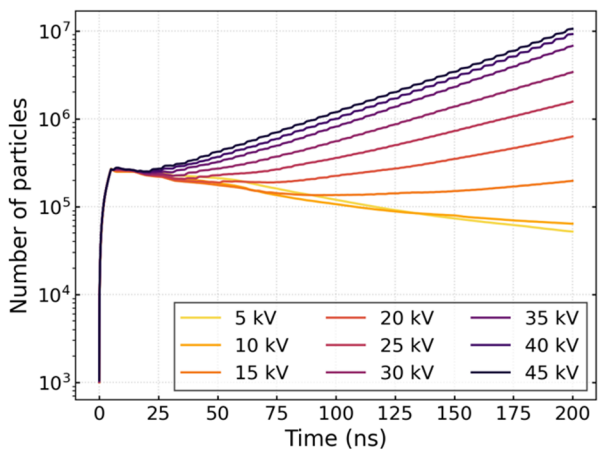

(c) $SEY_{peak} = 2.2$

Figure 7: Total number of particles as a function of time for Nb with different SEY curves.

ISBN: 978-3-95450-233-2 ISSN: 2673-5504 doi:10.18429/JACoW-SRF2021-TUPCAV015

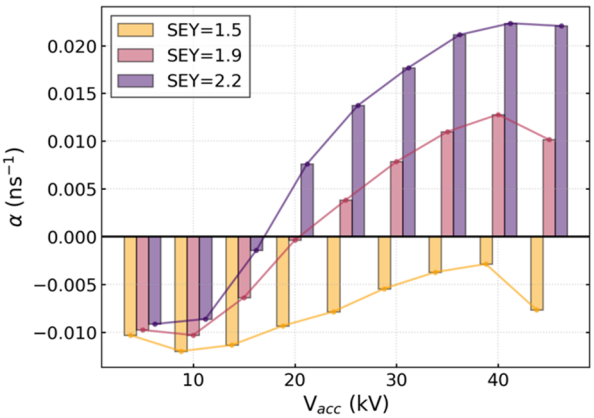

Figure 8: Exponential growth rate of number of particles as a function of accelerating voltage for Nb with different SEY curves.

Comparing to the experimentally measured MP barrier of 8 kV, the data imply a cavity surface condition having a high SEY curve (with a peak at 2.2 or higher), which may be related to the use of HPR with no vacuum baking afterwards [7].

Additionally, we noticed that the simulation time can affect the accurate determination of the particle growth rate. As shown in Fig. 9, if the simulation time cut off at 200 ns (Fig.7 (a)-(c)), the exponential growth rate suggests a negative increase (no multipacting). However, with the extended simulation time to over 2100 ns (420 rf periods), an obvious growing trend of total number of particles demonstrates a clear multipacting behavior showing up after ~48 rf cycles. The evolution of the secondary emitted particles can be found in Fig. 10. In the Fig. 10 (a)-(e), the emitted electrons were mainly originated from the coupler, the dome, and the toroid roundings; the overall negative growth behavior is likely related to the lowered number of electrons around the coupler regions. After the 48th rf period, the total number of generated secondary particles dramatically increases and spreads out to the whole cavity. By individual exponential fitting on the two regions (before 240 ns and after 240 ns), the calculated growth rates were found to be -0.0086 (same as the value in Fig. 8) and 0.0022 respectively. This 'delayed' growing trend deserves more systematic studies to understand whether this might be seen experimentally or whether it is due to, for example, the initial conditions of the MP simulation. In our case, this growth rate based on a longer simulation time implies a slightly lower MP turned-on voltage (<10 kV) than would be inferred from Fig. 8, which would be in good agreement with our experimental observation at 8 kV.

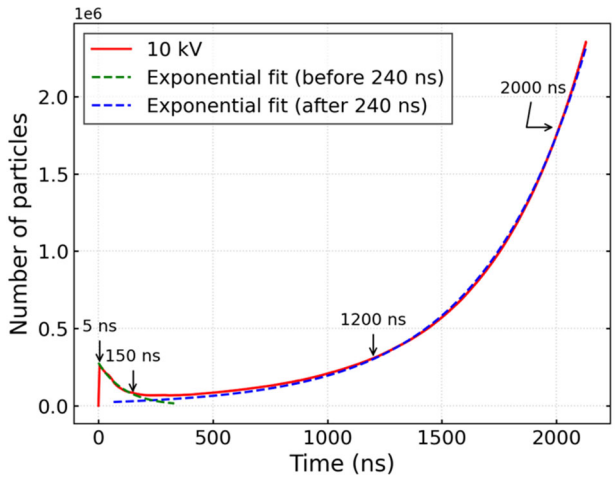

Figure 9: An example of the simulated number of particles as a function of time (V_{acc} = 10 kV, SEY_{peak} = 2.2).

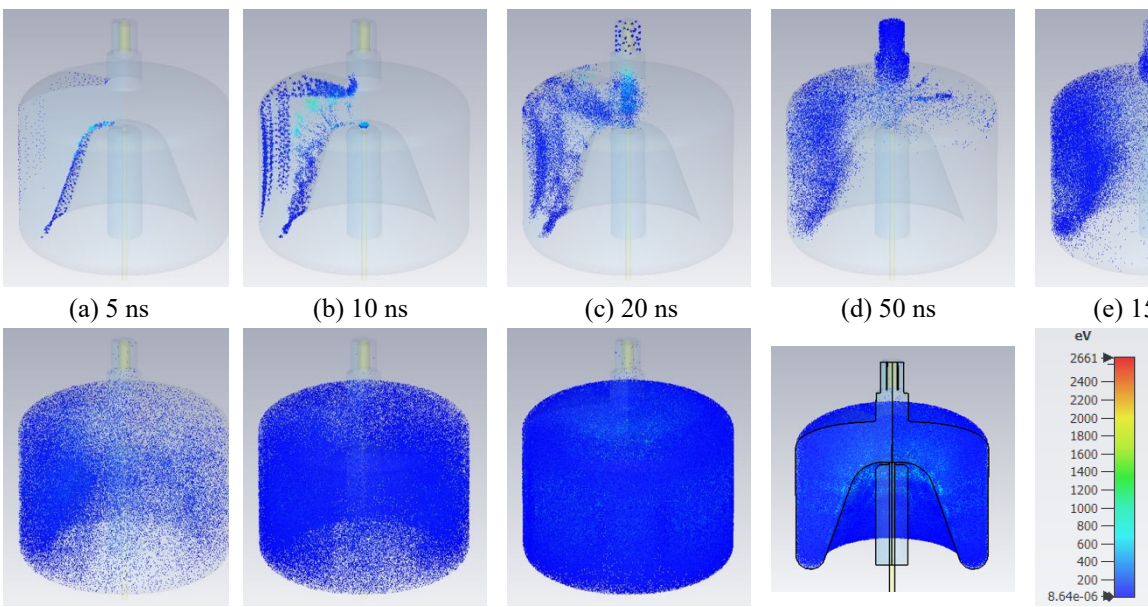

(a) 5 ns (b) 10 ns (c) 20 ns (d) 50 ns (e) 150 ns

(f) 500 ns (g) 1200 ns (h) 2000 ns (i) crossection view of (h)

Figure 10: Evolution of the secondary emitted particles in the cavity (V_{acc} = 10 kV, SEY_{peak} = 2.2).

ISBN: 978-3-95450-233-2 ISSN: 2673-5504 doi:10.18429/JACoW-SRF2021-TUPCAV015

FUTURE STUDY

Based on the MP simulations, secondary emitted particles were also found at higher accelerating voltage than the experimentally observed 40 kV. However, during the experiment, after breaking through the MP barrier at 40 kV, the accelerating voltage can be easily pushed to the measured maximum voltage of ~1 MV within a few minutes. Though a few numbers of MP were showed up at higher voltage level, those can be conditioned off in less than one minute. More systematic simulations are desired to reveal the detailed MP behavior in the cavity.

CONCLUSION

The field performance of WiFEL cavity was characterized. Q_0 was found to be 2.3×10^8 at the highest stable CW peak gradient of 15 MV/m. The strong experimentally observed multipacting effect was studied using CST. A good agreement on the MP turn-on voltage has been found between the CST simulation and the experimental results. Based on the simulation, the cavity may have a higher SEY which could likely be improved via cavity vacuum baking.

ACKNOWLEDGEMENTS

This work was supported by the U.S. Department of Energy, Office of Nuclear Physics, under Contract No. DE-AC02-06CH11357. This research used resources of ANL's ATLAS facility, which is a DOE Office of Science User Facility.

REFERENCES

[1] CST Studio Suite, version 2020, https://www.cst.com

[2] L. Cultrera *et al.*, "Cold electron beams from cryocooled alkali antimonide photocathodes", *Phys. Rev. ST Accel. Beams*, vol. 18, p. 113401, 2015. https://doi.org/10.1103/PhysRevSTAB.18.113401

[3] T. Petersen *et al.*, "Refurbishment and Testing of the WiFEL E-Gun at Argonne", presented at the 2021 Int. Conf. RF Superconductivity (SRF'21), East Lansing, Michigan, June-July 2021, virtual conference, paper WEPCAV015, this conference.

[4] I. Petrushina *et al*., "Mitigation of multipacting in 113 MHz superconducting rf photoinjector", *Phys. Rev. Accel. Beams*, vol. 21, p. 082001, 2018. https://doi.org/10.1103/PhysRevAccelBeams.21.082001

[5] E. L. Garwin *et al*., "Secondary electron yield and Auger electron spectroscopy measurements on oxides, carbide, and nitride of niobium", *J. Appl. Phys*., vol. 59, p. 3245, 1986. https://doi.org/10.1063/1.337046

[6] N. Hilleret *et al*., "The secondary-electron yield of air-exposed metal surfaces", *Appl. Phys. A*, vol. 76, p. 1085, 2003. https://doi.org/10.1007/s00339-002-1667-2

[7] S. Aull, T. Junginger, H. Neupert, and J. Knobloch, "Secondary Electron Yield of SRF Materials", in *Proc. 17th Int. Conf. RF Superconductivity (SRF'15)*, Whistler, Canada, Sep. 2015, paper TUPB050, pp. 686-690.